Chemical Engineering Science 164 (2017) 270–278

Contents lists available at ScienceDirect

Chemical Engineering Science

journal homepage: www.elsevier.com/locate/ces

Entrained droplets in two-phase churn flow

Ke Wang [a,b], Jing Ye [b,c], Bofeng Bai [b,*]

[a] Beijing Key Laboratory of Process Fluid Filtration and Separation, China University of Petroleum, Beijing 102249, China
[b] State Key Laboratory of Multiphase Flow in Power Engineering, Xi'an Jiaotong University, Xi'an 710049, China
[c] Shanghai Marine Diesel Engine Research Institute, Shanghai 201108, China

HIGHLIGHTS

- A shadow detection was developed to obtain the sharp pictures of entrained droplets.
- The liquid distribution in churn flow was investigated.
- The detailed process of the entrainment was discussed.
- An empirical formula was proposed to predict the droplet size.
- The relationship between the droplet size and the mechanism of the entrainment was analyzed.

ARTICLE INFO

Article history:
Received 7 December 2016
Received in revised form 6 February 2017
Accepted 16 February 2017
Available online 20 February 2017

Keywords:
Two-phase flow
Churn flow
Entrainment
Droplets

ABSTRACT

The presence of droplets exerts a strong influence on liquid film flow rate, pressure drop, heat transfer and many other flow characteristics. Due to the complexity of churn flow, profound knowledge on the droplets in this flow pattern is not well documented in the existing literature. In the present paper, we study a gas-liquid two-phase churn flow in a 19-mm-inner-diameter pipe under atmospheric pressure and carefully design a shadow detection technique to capture the high-resolution images of the entrained droplets in churn flow. The images are subsequently binarized using an adaptive threshold. The results indicate that the amount of the entrained droplets is high in the chaotic churn flow regime and gradually decreases during the transition from churn flow to annular flow and finally reaches a minimum around the churn-annular flow transition. The detailed process of the droplet entrainment is discussed. Based on our experimental observations, it is concluded that the large droplets (chunks) are related to the breakdown of slugs and bag breakup mechanism, whereas the smaller droplets can be ascribed to the breakup of chunks, ligament breakup and impingement. A normalized size probability density function is implemented to analyze the effect of the entrainment mechanism on the range of droplet size. The Sauter diameter of the droplets in churn flow is compared with the existing empirical correlations in annular flow and a formula for the entrained droplet size in churn flow is proposed.

1. Introduction

Entrainment is of great concern for the design of industrial processes. A profound understanding of the entrainment and entrained droplets is of utmost importance for the calculation of pressure drop, the determination of film flow rate and the prediction of heat transfer (Azzopardi and Zaidi, 2000; Sawant et al., 2009; Cioncolini and Thome, 2010). Excessive liquid entrainment, particularly in nuclear power plants, will cause the complete removal of the liquid film from the wall (dryout), resulting in disastrous accidents (Okawa et al., 2003). Recent research results indicate that the entrained droplets with great momentum generated in the churn flow regime are more likely to travel into the annular flow (Ahmad et al., 2010; Wang et al., 2014). This so-called “memory effect” will significantly change the phase distribution of the annular flow and thus cause errors in CHF prediction.

Most of the published work concentrates on the entrainment and entrained droplets in annular flow (Azzopardi, 1985; Fore and Dukler, 1995; Simmons and Hanratty, 2001; Westende et al., 2007; Berna et al., 2015a; Zhang et al., 2015). According to their experimental observations, Ishii and Grolmes (1975) proposed five basic types of entrainment mechanisms, i.e. roll wave, wave undercut, bubble bursting, liquid impingement and liquid bulge disintegration. Based on the force balance of the hydrodynamic and the surface tension forces, previous theoretical studies provided detailed analysis of the effect of the relevant parameters on entrainment in annular flow (Holowach et al., 2002; Ryua and Park, 2011).

* Corresponding author.
E-mail address: bfbai@mail.xjtu.edu.cn (B. Bai).

http://dx.doi.org/10.1016/j.ces.2017.02.028
0009-2509/

Nomenclature

a	width of the divided size classes
d_i	droplet diameter (μm)
d_{32}	Sauter diameter (μm)
D	pipe inner diameter (m)
M_l	liquid mass flow rate (kg/s)
Re	Reynolds number
t	time (s)
u_{sg}	gas superficial velocity (m/s)
u_{sl}	liquid superficial velocity (m/s)
U_g^*	dimensionless gas velocity
We	Weber number

Greek letters

ρ	density (kg/m^3)
σ	surface tension (N/m)
μ	viscosity (kg/m·s)

Subscripts

g	gas
l	liquid

Azzopardi (1997) systematically summarized the available studies on the droplet in annular flow, providing insights into its generation (atomization or entrainment), existence (size and motion) and removal (re-deposition). Later, Berna et al. (2015b) provided a more detailed review of the characteristics of the entrained droplet (including its generation, size, speed and total amount, etc.) and proposed new correlations for its size and amount. Nevertheless, research findings about the droplet in churn flow are lacking. As we know, churn flow appears a highly oscillatory liquid film accompanied by a continuous gas core with considerable amount of entrained liquid. Generally, the liquid oscillation and violent fluctuation of pressure gradient as well as the liquid holdup are due to the movement reversal of huge waves and their eventual breakup into droplets of various sizes (Jayanti and Hewitt, 1992; Hewitt et al., 1985; Owen, 1986). Some of the experimental work available studied the structure of gas-liquid interface (Sharaf et al., 2015; Parsi et al., 2015a, b; Parsi et al., 2016), the properties of interfacial waves (Barbosa et al., 2001; Wang et al., 2012, 2013a; Tekavčič et al., 2016), the mechanism of entrainment (Barbosa et al., 2002; Wang et al., 2013b) and the entrained fraction (Barbosa et al., 2002) under this circumstance. The switch from bag breakup to ligament breakup consequently yields that the entrained fraction is high in chaotic churn flow and gradually diminishes to a minimum at the churn-annular flow transition and increases in annular flow thereafter. A general understanding of the generation of droplets in churn flow has been concluded, but the investigation on the droplet size distribution is not widely available. It is probably because the conventional measurement for droplets in annular flow could induce significant errors in the churn flow scenario. Due to its chaotic nature, it is not possible to remove the liquid film without causing significant disturbance to the flow. Equally, it is impossible to get close to the source of the entrainment, namely, the huge waves from which the droplets are generated.

The present study investigates the entrained droplets under churn flow condition. We use a high-resolution camera to capture the more detailed liquid distribution in the cross-section of the tube. We also analyze the effects of different parameters (e.g. gas and liquid flow rate) on the phase distribution. Based on the entrainment mechanism analysis, we discuss the generation and size distribution of the droplets and proposed an empirical correlation based on the existing correlation in annular flow, providing insights into the differences between churn flow and annular flow.

2. Experiment method

2.1. Test facility

Fig. 1 shows the schematic of the test facility which mainly consists of water and air supply systems, a test section as well as a measurement system. The test section is a transparent acrylic tube with the inner diameter of 19 mm and the height of 2 m Porous walls in the mid and lower part of the tube are delicately designed for the air-water mixture and water extraction. The Nikon D700 digital camera with a Sigma150 mm f/2.8 Macro Lens is placed facing the outlet of the tube to capture the high-resolution images of the entrained droplets with the sample rate of 5 pictures/s. A flash synchronization connected to the camera is used to illuminate the background of the moving droplets. In order to prevent the droplets from contaminating the lens and obscuring the view, the side wind blows the droplets immediately into a water collector when they flow out of the pipe.

2.2. Experimental method and procedures

The detailed experimental procedures to obtain churn flow are accessible in our previous paper (Wang et al., 2013a). Huge waves repeatedly form in the water inlet region and then fluctuate with the gas flow on the falling film. During the moving process, they break up into droplets (undercut or sheared off). In the present study, the flow conditions vary from churn flow to annular flow. The gas volume flow V_g ranges from 5.0 m^3/h to 13.0 m^3/h and the liquid mass flow M_l from 1.63×10^{-2} kg/s to 2.49×10^{-1} kg/s. It is noted that all the experiments are carried out under atmospheric pressure and room temperature. For the sake of the highly desirable pictures of the entrained droplets, the results from three

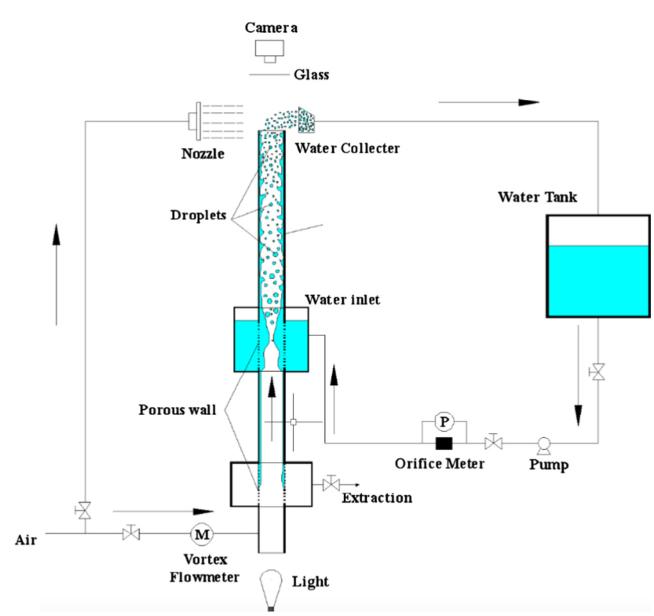

Fig. 1. Schematic of the test facility.

different shootings are presented and compared in the present paper, as seen in Fig. 2. When the illuminated plane and the focal plane are on the same plane (Fig. 2a), most of the droplets are overexposed and cannot be easily recognized due to the strong reflection. When the illuminated plane is placed a certain distance behind the confocal plane (say, 5 mm in Fig. 2b), the background of the droplets is lightened and the edge of the large droplets is easily detected. However, the droplets of small size, in particular, are impossible to be distinguished from the environment because of their transparency. Therefore, the droplets have to be highlighted against the background in order to be clearly captured. Our present study makes use of the droplet shadow for their detection. In Fig. 2c, the droplets are placed in the optical path between the light source and the camera, so their shadows (the dark blobs) are quite visible in the cross-section of the tube. It is noted that the whole tube is covered by the aluminum foil to prevent the light from escaping. Fig. 2c presents the shadows of the in-focus droplets (the sharp edge) and the shadows of the out-of-focus droplets (the diffuse edge). Accordingly, by detecting the shadows of the droplets, the entrained droplets of various sizes can be captured. Note that this detection will not work well for droplets of higher concentration as the plethora of droplets can obscure the light beams, adversely affecting the measurements.

2.3. Data processing

In order to improve the droplet identification, binarization of images by Matlab is applied to recognize each of the blobs. It should be noted that the liquid film distributed along the circumference of the tube is removed first. The blobs are identified as the droplets when they satisfy the sharpness criterion (the in-focus droplets). By applying the adaptive threshold to the intensity image, a binary image with two values, one for the droplets and the other for the background (the pure gas) is concluded. The droplets have an intensity value below 25 and the background between 25 and 255 (see Fig. 3). Remarkably, the binarization not only gets rid of the undesired objects or impurities, but also provides a sharp contrast between the blobs and the background. In terms of the binary image, the droplet size is calculated by image processing software Image-J, version 1.51e (Ferreira and Rasband, 2012. The ImageJ User's Guide. Available at https://imagej.nih.gov/ij/docs/guide [accessed on January 15, 2017]).

2.4. Uncertainty analysis

The water flow is measured by an orifice mass flux meter with the uncertainty of 0.5%, and the pressure drop by a Rosemount

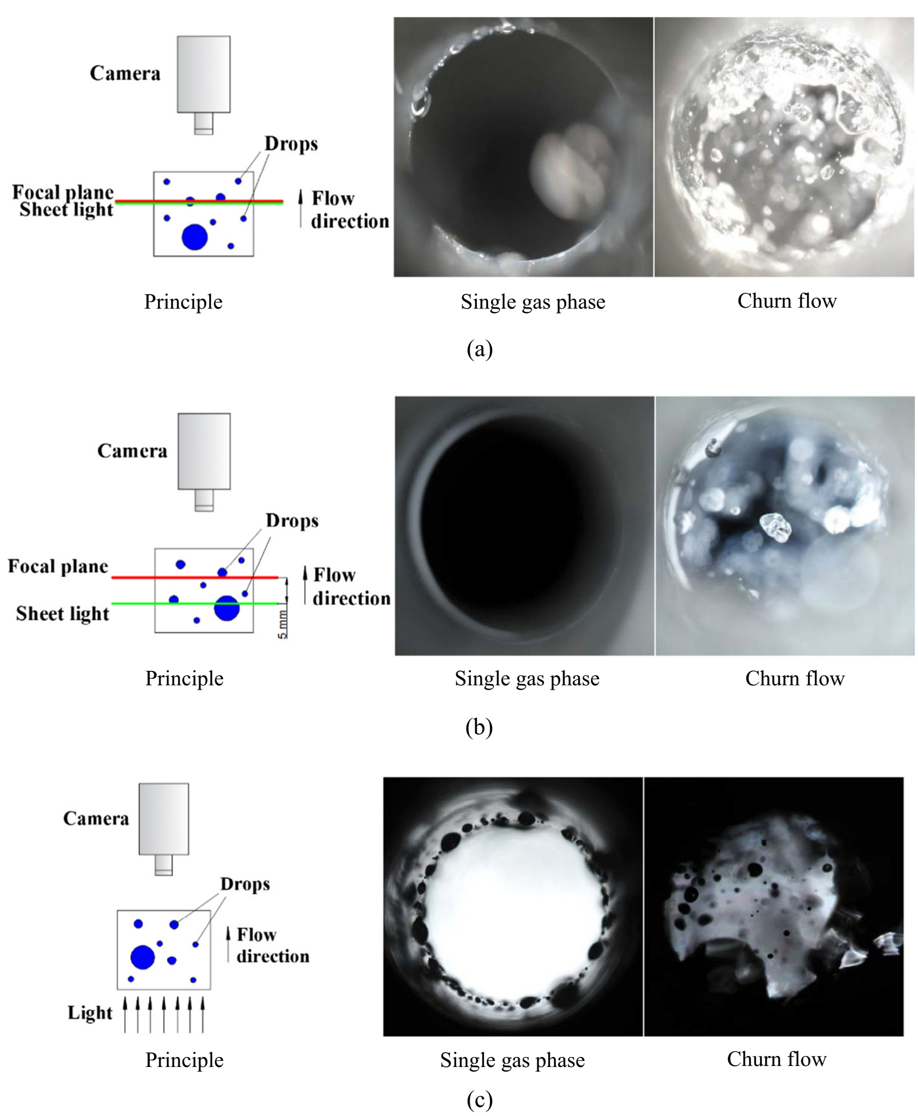

Fig. 2. Methods for capturing droplets.

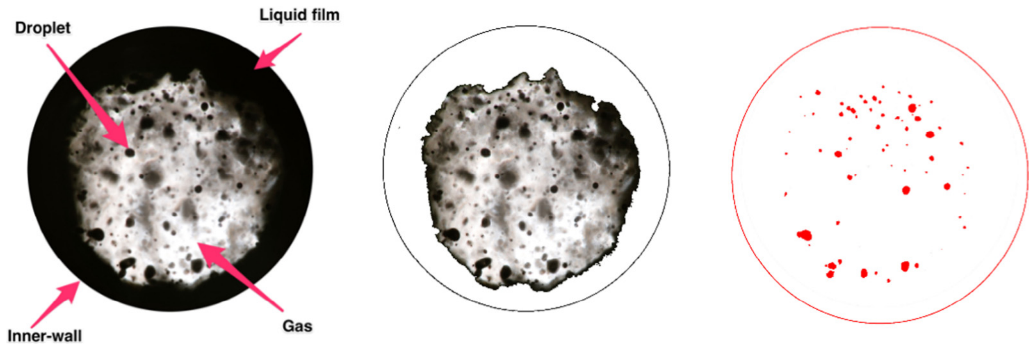

(a) Original (b) Liquid film removed (c) Droplets detected

Fig. 3. Droplet identification.

3051 transmitter with the uncertainty of ±0.5% and the air flow by a rotameter with accuracy grade of 1.0 classes. The distribution of the droplets varies in time and space, particularly in the chaotic churn flow, which indicates that the detection of the droplets is not always following the same protocol (photography, laser anemometry, probe, etc.) and will lead to the diversity in the results. Evidently, to obtain the accurate droplet size distribution or mean diameter requires either a very large number of droplets or reliable statistics of the droplets. Additionally, the binarization inevitably induces loss of some data. Thus, the data of the entrained droplets in the present paper is an accumulative (collective) parameter obtained during a specific period. In our study, for a fixed flow condition, about 30 pictures are selected, i.e., more than 3000 droplets are analyzed to redeem the loss of the data. It is noteworthy that the overlapping droplets are artificially split and the measurement is based on the assumption that the droplets are spherical. Large droplets or chunks, in particular, are observed to be non-spherical and would thus be treated as equivalent spherical particles.

Therefore, the sensitivity of the droplet detection in the present study depends on the resolution of the pictures and the non-circularity of the droplets. In the present study, the resolution of the pictures applied in Image-J is 300 ppi and the non-circularity is stochastic. According to the theory of error propagation, the error of d_{32} can be obtained. Taking the flow condition u_{sl} = 0.08 - m/s and u_{sg} = 12.7 m/s for example, the error of d_{32} calculated is about 7%, which is reasonable and agrees with the data shown in Azzopardi (1997).

3. Results and discussion

3.1. Spatial distribution of droplets

Fig. 4 shows the liquid distribution in the cross-section of the tube from churn flow to annular flow. In general, the liquid distribution and the generation of droplets are random. After the breakdown of slug flow, the liquid distribution in the churn flow regime is characterized as highly chaotic, i.e. the extremely thick liquid film plus the plethora of droplets (the majority of the chunks) occupies nearly the whole tube (Fig. 4a). By increasing the gas velocity, the thickness of the liquid film gradually decreases, whereas the oscillation in the liquid film leads to the irregular distribution and protrusions into the gas core. Apparently, the amount of the entrained liquid also decreases. When it is close to the transition to annular flow, the fluid film is comparatively thin and uniformly spreads about the tube circumference. Few small- sized droplets are observed in the gas core, indicating a fraction of minimum entrained droplets. Similar conclusions were drawn from the work of Barbosa et al. (2002). The generation of large droplets (chunks) slows down with the increasing gas velocity whereas small droplets start to appear in mass (Fig. 4b and c), thus a decrease in mean droplet diameter. It can be concluded that the effect of the bag breakup mechanism is more prominent for lower gas velocity and for higher gas velocity the effect of the filament breakup mechanism is more dominant. Additionally, large droplets are more likely to aggregate and deposit instantly on the liquid film, while the smaller droplets are misty.

3.2. Mechanism of droplet generation

It is commonly considered that churn flow occurs after the breakdown of slug flow and the flooding of the fluid film is attributed to the transition from slug flow to churn flow. Huge waves and the subsequent disturbance waves periodically form and travel on the falling liquid film and finally break up into droplets of various sizes. According to our observations, three main mechanisms for droplet generation are illustrated in Fig. 5. In the slug-churn flow transition, with an increase in gas flow rate, the Taylor bubble becomes seriously distorted. The liquid slug shrinks and finally collapses into liquid chunks. This breakdown of liquid slug results in a sudden acceleration and impels the chunks to break up into small droplets (see Fig. 5a). Subsequently, the falling liquid accumulates, forming the so-called huge wave, and is again broken up by the gas. Thus, the bag breakup (undercut) plays a dominant role at low gas superficial velocity (see Fig. 5b), whereas the ligament breakup (sheared-off) comes to gain greater importance with the increase of gas flow rate (see Fig. 5c). In the case of ligament breakup, the wave crest is "stretched" into the gas core (see the protrusion in Fig. 5c) and then sheared off by the coming gas flow. The filament subsequently breaks up into small droplets. Comparably, small droplets tend to stay in the core for much longer due to the turbulent eddy interactions within the gas core. In the case of bag breakup mechanism, an open-ended bubble is formed with a thick filament rim and the part of the wave is undercut to form a liquid chunk. The detailed process for this mechanism in the cross-section view is illustrated in Fig. 6. Subsequently, the chunk breaks up into smaller droplets or deposits instantly on the liquid film to cause a secondary entrainment (impingement) to generate smaller droplets. Note that it is impossible in the present study to capture the detailed process of the ligament mechanism in the cross-section of the tube. That is because the disturbance waves and the entrained droplets with higher velocities travel out of the focal plane very quickly.

3.3. Droplet size

Probability density functions (PDFs), which can be interpreted as normalized histograms, are created for each of the experiments

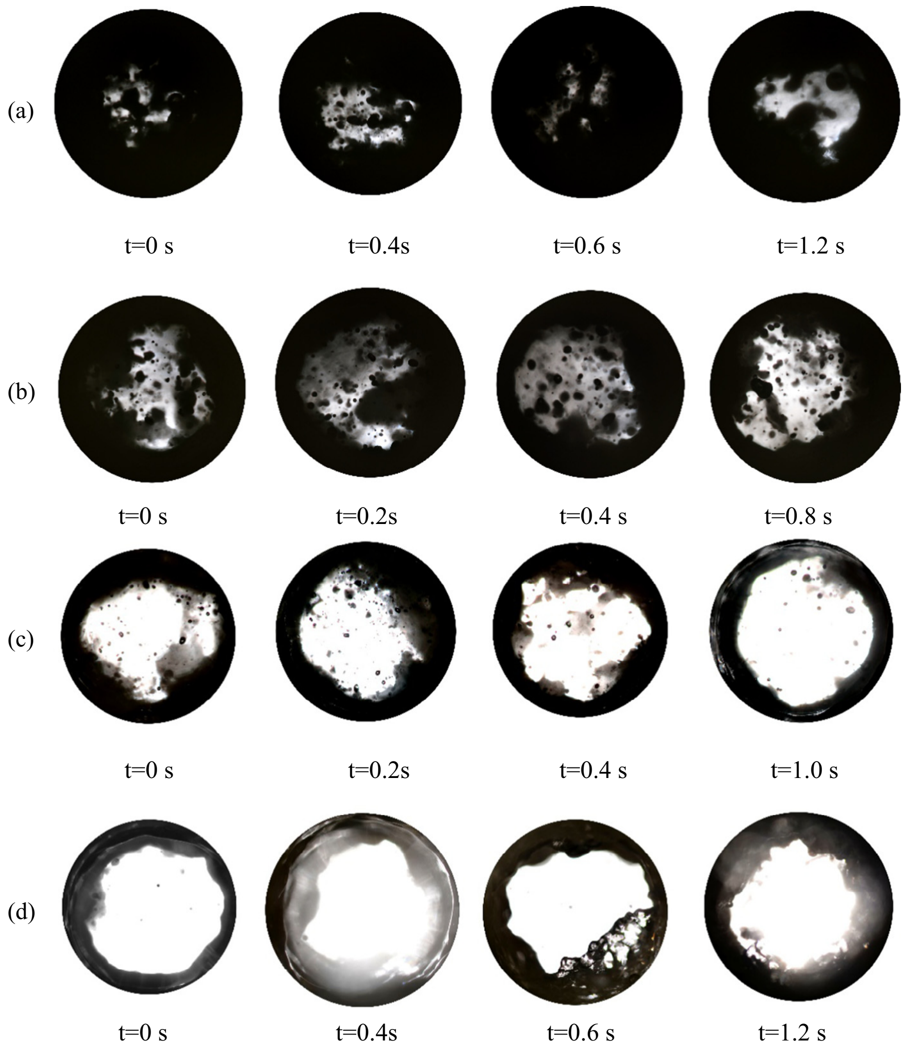

Fig. 4. Variations of the liquid distribution in the cross-section. D = 19 mm, $M_l = 2.42 \times 10^{-2}$ kg/s. (a) u_{sg} = 6.86 m/s, (b) u_{sg} = 9.47 m/s, (c) u_{sg} = 10.78 m/s, (d) u_{sg} = 12.73 m/s.

distinguishing the droplet data with a functionality with respect to the droplet diameter. The size probability density of the droplets can be estimated as follows,

$$PDF(d_i) = \frac{N_i}{N \cdot a} \tag{1}$$

where a is the width of the divided size classes, d_i is the droplet diameter, N_i is the droplet number in the range of $d_i \pm a$ and N is the total droplet number.

Fig. 7 shows the size distribution histograms for different liquid mass flow rates but the same gas superficial velocity. It should be noted that the size class width is set to 50 μm. When the flow regime is a typical churn flow, the entrainment is dominated by the bag breakup and large droplets (maxima 2400 μm) can be clearly indicated on the PDFs (see Fig. 7a and b). By decreasing the liquid mass flow rate, the generation of the huge wave subsides, resulting in the droplets ceasing to be generated due to the undercutting mechanism and gradual disappearance of large droplets in PDF (see Fig. 7c). With the further decrease of the liquid mass flow rate, the ligament breakup mechanism governs the entrainment and the droplets formed thereby are misty. In the transition from churn flow to annular flow, the distribution is more like that in annular flow (see Fig. 7d).

Fig. 8 shows the size cumulative distribution of the entrained droplet, which can be calculated by,

$$F_d(d_i) = a\sum_{i=1}^{N} PDF(d_i) \tag{2}$$

Take the growth rate of size cumulative distribution near the churn-annular flow transition for comparison purpose. Increasing liquid mass flow rate firstly leads to the appearance of a large number of droplets with relatively small size and uniform distribution. However, due to the competitive relationship between the undercutting mechanism and shear-off mechanism, further increasing liquid mass flow rate consequently results in the generation of liquid chunks. Compared with the region close to annular flow, droplets with a wider range of size can be found in the early stage of churn flow, which demonstrates that the mechanism of droplet generation in churn flow is more complicated than that in annular flow. Note that the distribution curve at u_{sl} = 0.08 m/s lies below the u_{sl} = 0.17 m/s curve. The cause remains uncertain, but according to Fig. 7d, it is supposed that the number of droplets with small diameter (<200 μm increases and their distribution appears more uniform when the liquid mass flow rate is lower. It indicates that the bigger droplets break up into smaller ones and the transition from churn flow to annular flow is approaching. In addition, the smaller droplets (<10 μm) present in the gas core cause the flow image at higher gas velocity to become more “misty”. Due to the limit of the resolution, it is difficult to distinguish these droplets, resulting in a bigger calculation error.

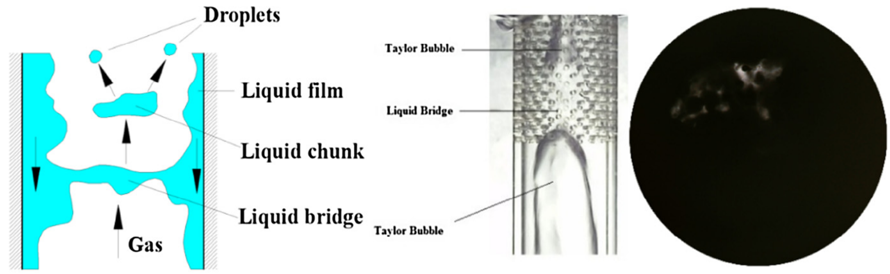

Principle (Ishii and Grolmes, 1975) Axial (Wang et al., 2013a) Cross-section

(a) Bridge break down

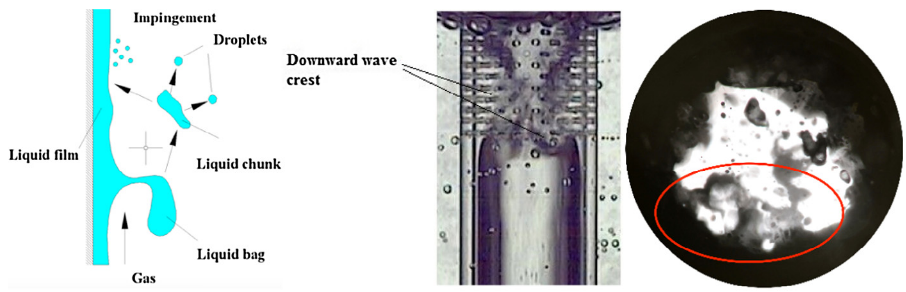

Principle (Ishii and Grolmes, 1975) Axial (Wang et al., 2013a) Cross-section

(b) Bag breakup and droplet impingement

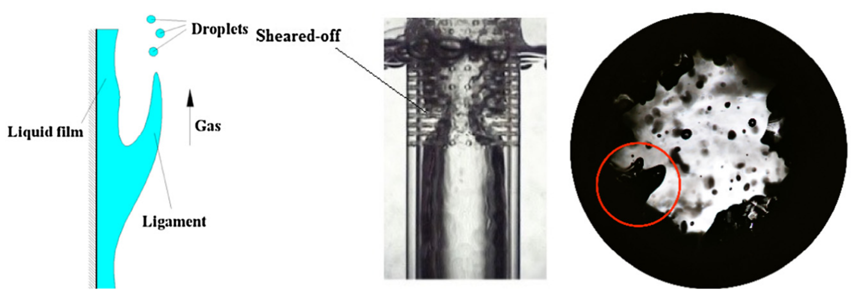

Principle (Ishii and Grolmes, 1975) Axial (Wang et al., 2013a) Cross-section

(c) Ligament breakup

Fig. 5. The mechanisms of droplet generation.

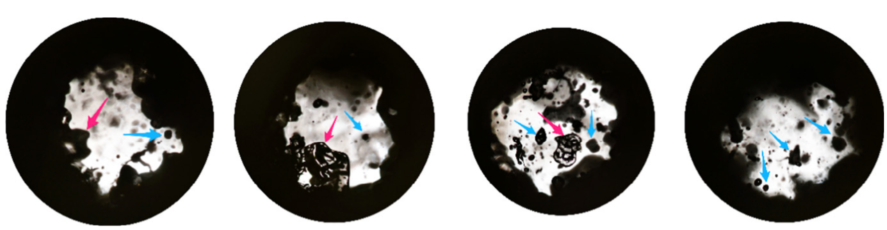

t=0 s t=0.2s t=0.4 s t=0.8 s

Fig. 6. The detailed process of bag breakup. D = 19 mm, $M_l = 2.42 \times 10^{-2}$ kg/s, u_{sg} = 8.82 m/s.

3.4. Comparison with droplet size correlations in annular flow

The empirical correlations for droplet size in annular flow have been well documented in the literature, but seldom for churn flow. Here, some typical correlations which describe the Sauter diameter (d_{32}) in annular flow, are used for the comparison in order to illustrate the characteristics of churn flow, as listed in Table 1.

The comparisons of the current experimental data with the existing empirical expressions are shown in Fig. 9. It is indicated that Kim's and Al-Sarkhi and Hanratty's correlations fail to predict

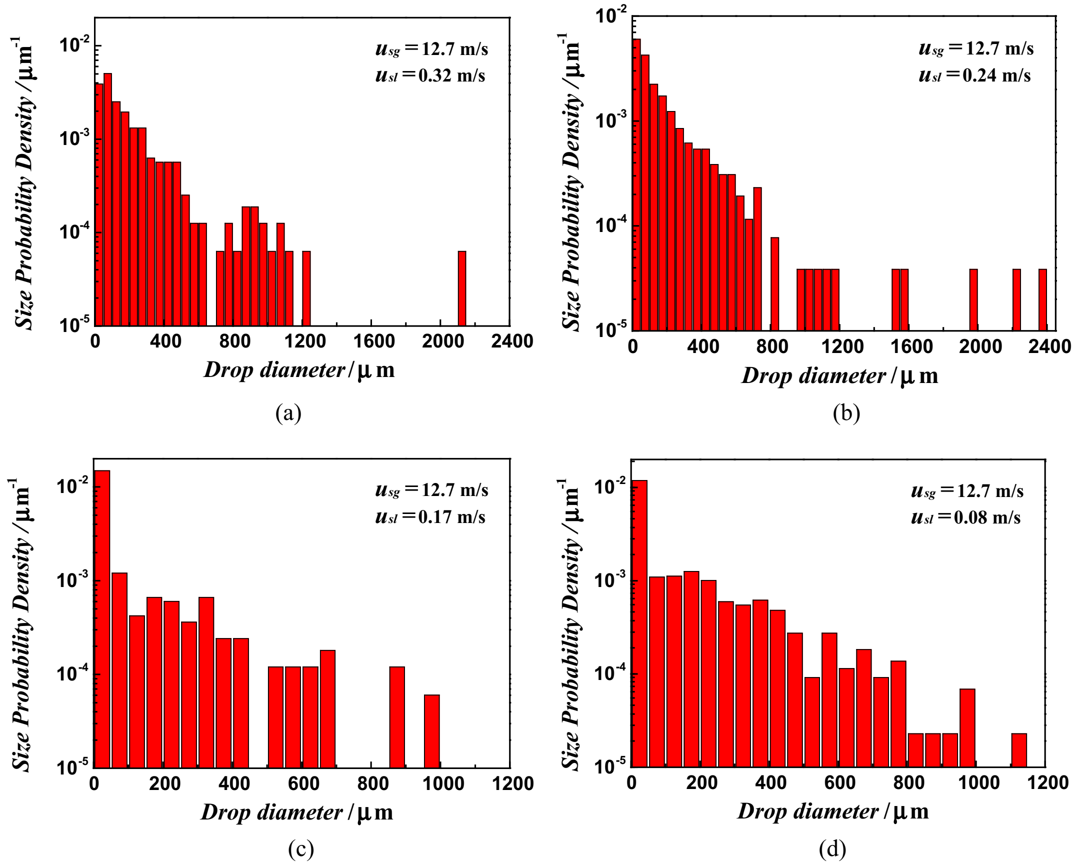

Fig. 7. Size probability density distributions.

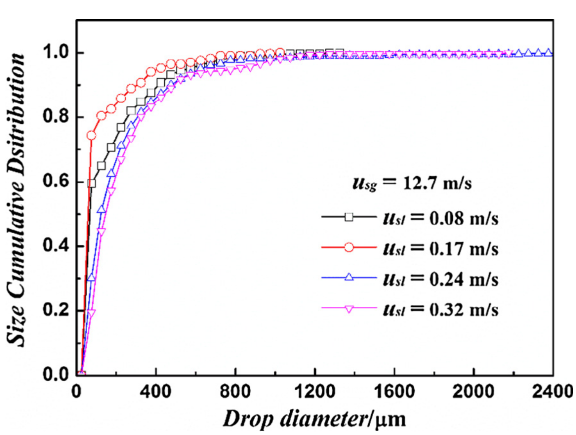

Fig. 8. Size cumulative distribution.

Table 1
Typical correlations for droplet size prediction in annular flow.

References	Empirical correlations
Kim et al. (1993)	$\frac{d_{32}}{D} = 0.00796\frac{Re_{sg}^{2/3}}{We_{sg}}\left(\frac{\rho_g}{\rho_l}\right)^{-\frac{1}{3}}\left(\frac{\mu_g}{\mu_l}\right)^{\frac{2}{3}}$ (3) where $We_{sg}, Re_{sg}, D, \rho_g, \rho_g, \mu_g, \mu_l$ and σ are gas phase Weber number ($We_{sg} = \rho_g u_{sg}^2 D/\sigma$), gas Reynolds number ($Re_{sg} = \rho_g u_{sg} D/\mu_g$), pipe diameter, gas and liquid density, gas and liquid viscosity and surface tension, respectively
Al-Sarkhi and Hanratty (2002)	$\frac{d_{32}}{D} = D^{-1}\left[0.154D^{0.36}\left(\frac{\rho_g u_{sg}^2}{\sigma}\right)^{-0.55}\right]^{1.0989} = 0.128We_{sg}^{-0.604}$ (4)
Azzopardi (2006)	$\frac{d_{32}}{D} = \left[0.069u_{sg} + 0.0187\left(\frac{\rho_l u_{sl}}{\rho_g u_{sg}}\right)^2\right]\frac{1}{We_{sg}}$ (5)

the droplet diameter, particularly in the early stage of churn flow. That is, their correlations overestimate or underpredict the experimental data in the present study. Note that the miscalculation apparently becomes less pronounced at higher gas velocity since the flow pattern changes from churn flow to annular flow. Comparatively, the correlation proposed by Azzopardi has a fair estimation of the current data in churn flow.

The root-mean-square error (RMSE) is also employed to evaluate the correlations, as shown in Table 2. Though the equations proposed by Kim et al. (1993) and Al-Sarkhi and Hanratty (2002) seem more accurate than the equation proposed by Azzopardi (2006), they only take the effect of gas phase into account. Azzopardi's equation shows a relatively complex dependence on gas and liquid flow rate and physical properties, which is more suitable for the ranges of the parameters in industrial applications. Accordingly, based on the regression analysis, the Azzopardi's correlation can be modified with the experimental data by introducing a correction factor to fit the churn flow condition, as seen in Fig. 10.

$$\frac{d_{32}}{D} = 0.5934\left(U_g^{*1.74}\right)f\left(\frac{d_{32}}{D}\right)_{\text{Azzopardi}} \quad (6)$$

$$U_g^* = u_{sg}\sqrt{\frac{\rho_g}{gD(\rho_l - \rho_g)}} \quad (7)$$

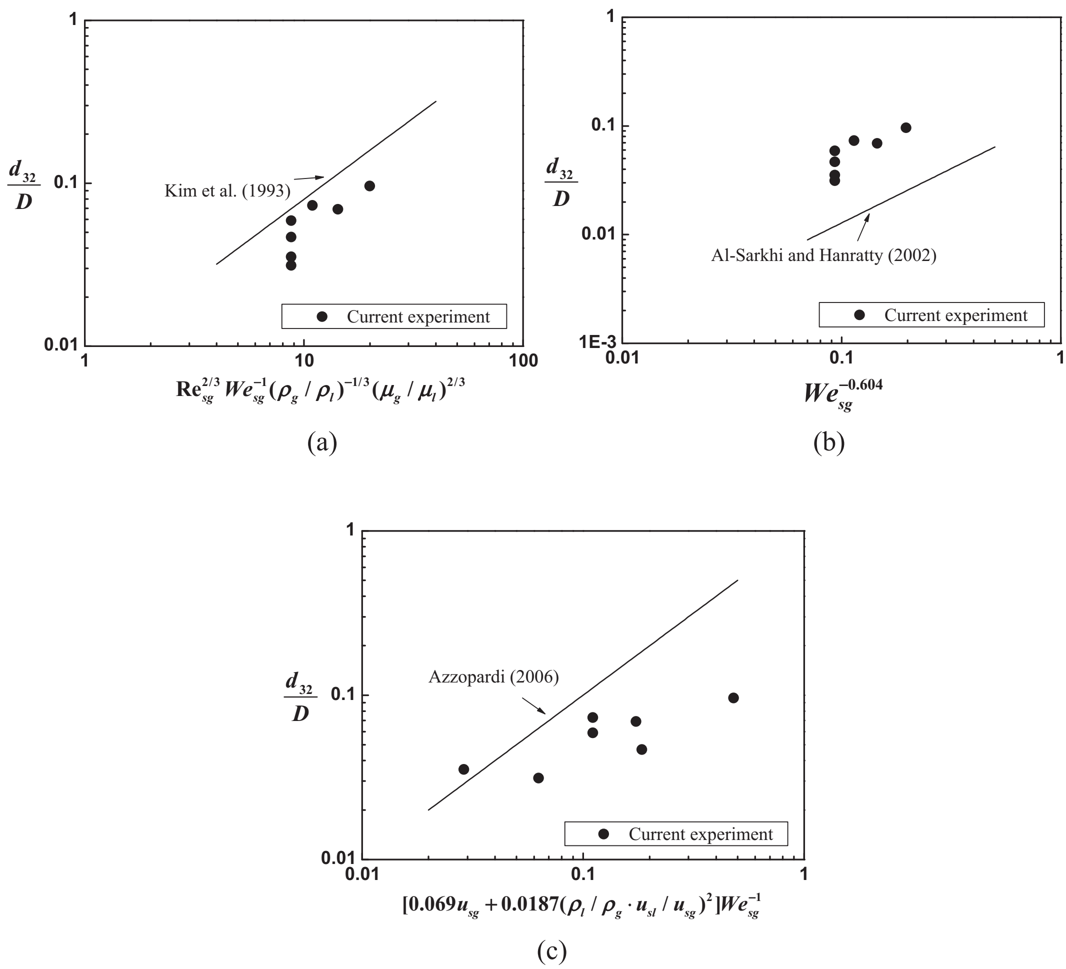

Fig. 9. Comparison of d32 of the droplets with empirical correlations for annular flow.

Table 2
Root-mean-square error of different correlations.

Source	Graph	RMSE (%)
Kim et al. (1993)	Fig. 9(a)	3.7
Al-Sarkhi and Hanratty (2002)	Fig. 9(b)	4.8
Azzopardi (2006)	Fig. 9(c)	16.1
Present work	Fig. 10	2.8

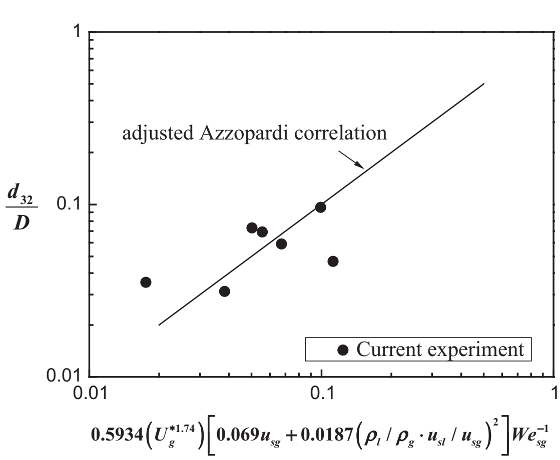

Fig. 10. Modified correlation for droplet size prediction in churn flow.

4. Conclusion

The present study investigates the generation and size distribution of entrained droplets under churn flow condition in a vertical pipe with the inner diameter of 19 mm. The distribution of liquid phase and the detailed process for the generation of droplets are discussed thoroughly. Due to the competitive relationship between the bag breakup mechanism and ligament breakup mechanism, the generation of large droplets (chunks) slows down with the increasing gas velocity whereas small droplets start to appear in mass, thus a decrease in mean droplet diameters. Additionally, large droplets are more likely to aggregate and deposit instantly on the liquid film, while the smaller droplets are misty. We also employ the normalized size probability density function to demonstrate the effect of entrainment mechanism on droplet generation. By comparison with the existing empirical correlations in annular flow, we modify the size prediction proposed by Azzopardi to fit the churn flow condition, which is subject to further verification with massive experimental data in the future work.

Acknowledgments

The authors gratefully acknowledge research support from the National Natural Science Foundation of China under Grant No. 51276140, 51474229 and the Science Foundation of China University of Petroleum, Beijing No. 2462016YJRC029.

References

Ahmad, M., Peng, D. J., Hale, C. P., et al., 2010. Droplet Entrainment in Churn Flow, International Conference of Multiphase Flow, Florida, USA.
Al-Sarkhi, A., Hanratty, T.J., 2002. Effect of pipe diameter on the drop size in a horizontal annular gas-liquid flow. Int. J. Multiphase Flow 28, 1617–1629.
Azzopardi, B.J., 1985. Drop-sizes in annular two-phase flow. Exp. Fluids 3, 53–59.
Azzopardi, B.J., 1997. Drops in annular two-phase flow. Int. J. Multiphase Flow 23 (7), 1–53.
Azzopardi, B.J., Zaidi, S.H., 2000. Determination of entrained fraction in vertical annular gas/liquid flow. J. Fluid Eng. – Trans. ASME 122 (1), 146–150.
Azzopardi, B.J., 2006. Gas-Liquid Flows. Begell House Inc., New York.
Barbosa, J., Govan, A.H., Hewitt, G.F., 2001. Visualization and modeling studies of churn flow in a vertical pipe. Int. J. Multiphase Flow 27 (12), 2105–2127.
Barbosa, J.R., Hewitt, G.F., König, G., et al., 2002. Liquid entrainment, droplet concentration and pressure gradient at the onset of annular flow in a vertical pipe. Int. J. Multiphase Flow 28 (6), 943–961.
Berna, C., Escriva, A., Munozcobo, J.L., et al., 2015a. Review of droplet entrainment in annular flow: interfacial waves and onset of entrainment. Prog. Nucl. Energy 74, 14–43.
Berna, C., Escriva, A., Munozcobo, J.L., Herranz, L.E., 2015b. Review of droplet entrainment in annular flow: characterization of the entrained droplets. Prog. Nucl. Energy 79, 64–86.
Cioncolini, A., Thome, J., 2010. Prediction of the entrained liquid fraction in vertical annular gas–liquid two-phase flow. Int. J. Multiphase Flow 36 (4), 293–302.
Ferreira, T., Rasband, W., 2012. ImageJUser Guide. National Institute of Mental Health, Bethesda, Maryland, USA.
Fore, L.B., Dukler, A.E., 1995. The distribution of drop size and velocity in gas-liquid annular flow. Int. J. Multiphase Flow 21 (2), 137–149.
Hewitt, G.F., Martin, C.J., Wilkes, N.S., 1985. Experimental and modelling studies of annular flow in the region between flow reversal and the pressure drop minimum. PhysicoChem. Hydrodyn. 6 (1/2), 69–86.
Holowach, M.J., Hochreiter, L.E., Cheung, F.B., 2002. A model for droplet entrainment in heated annular flow. Int. J. Heat Fluid Flow 23, 807–822.
Ishii, M., Grolmes, M.A., 1975. Inception criteria for droplet entrainment in two-phase concurrent film flow. AIChE J. 21, 308–318.
Jayanti, S., Hewitt, G.F., 1992. Prediction of the slug-to-churn flow transition in vertical two-phase flow. Int. J. Multiphase Flow 18 (6), 847–860.
Kim, B.H., Peterson, G.P., Khim, K.D., 1993. Analytical and experimental investigation of entrainment in capillary pumped wicking structures. J. Energy Resour. Technol. 115, 278–286.
Okawa, T., Kotani, A., Kataoka, I., et al., 2003. Prediction of critical heat flux in annular flow using a film flow model. J. Nucl. Sci. Technol. 40 (6), 388–396.
Owen, D.G., 1986. An experimental and Theoretical Analysis of Equilibrium Annular Flows Ph.D. Thesis. University of Birmingham, UK.
Parsi, M., Vieira, R.E., Torres, C.F., et al., 2015a. Experimental investigation of interfacial structures within churn flow using a dual wire-mesh sensor. Int. J. Multiphase Flow 72, 155–170.
Parsi, M., Vieira, R.E., Torres, C.F., et al., 2015b. On the effect of liquid viscosity on interfacial structures within churn flow: experimental study using wire mesh sensor. Chem. Eng. Sci. 130, 221–238.
Parsi, M., Agrawal, M., Srinivasan, V., et al., 2016. Assessment of a hybrid CFD model for simulation of complex vertical upward gas–liquid churn flow. Chem. Eng. Res. Des. 105, 71–84.
Ryua, S.H., Park, G.C., 2011. A droplet entrainment model based on the force balance of an interfacial wave in two-phase annular flow. Nucl. Eng. Des. 241, 3890–3897.
Sawant, P., Ishii, M., Mori, M., et al., 2009. Prediction of amount of entrained droplets in vertical annular two-phase flow. Int. J. Heat Fluid Flow 30 (4), 715–728.
Sharaf, S., Meulen, G.P.V.D., Agunlejika, E.O., et al., 2015. Structures in gas–liquid churn flow in a large diameter vertical pipe. Int. J. Multiphase Flow 78, 88–103.
Simmons, M.J., Hanratty, T.J., 2001. Droplet size measurements in horizontal annular gas-liquid flow. Int. J. Multiphase Flow 27 (5), 861–883.
Tekavčič, M., Končar, B., Kljenak, I., 2016. Simulation of flooding waves in vertical churn flow. Nucl. Eng. Des. 2016 (299), 214–224.
Wang, K., Bai, B.F., Cui, J.H., Ma, W.M., 2012. A physical model for huge wave movement in gas-liquid churn flow. Chem. Eng. Sci. 79 (10), 19–28.
Wang, K., Bai, B.F., Ma, W.M., 2013a. Huge wave and drop entrainment mechanism in gas-liquid churn flow. Chem. Eng. Sci. 104, 638–646.
Wang, K., Bai, B.F., Ma, W.M., 2013b. A model for droplet entrainment in churn flow. Chem. Eng. Sci. 104, 1045–1055.
Wang, K., Bai, B.F., Ma, W.M., 2014. An improved liquid film model to predict the CHF based on the influence of churn flow. Appl. Therm. Eng. 64 (1), 422–429.
Westende, J.M., Kemp, H.K., Belt, R.J., et al., 2007. On the role of droplets in cocurrent annular and churn-annular pipe flow. Int. J. Multiphase Flow 33 (6), 595–615.
Zhang, R., Liu, H., Liu, M., et al., 2015. A probability model for fully developed annular flow in vertical pipes: prediction of the droplet entrainment. Int. J. Heat Mass 84, 225–236.